Automatic Selection of Release Plane for Lagrangian-based Wind-driven Rain Studies

George Xu[a], Kendrick Tan[a,*], Zhengwei Ge[a], Hee Joo Poh[a], Chin Chun Ooi[a], Yong Eng[b]

[a] *Institute of High Performance Computing, Agency for Science, Technology and Research (A*STAR), 1 Fusionopolis Way, #16-16 Connexis, Singapore, 138632, Singapore*
[b] *Building & Research Institute, Housing Development Board, HDB Hub, 480 Lorong 6 Toa Payoh, Singapore, 310480, Singapore*

Abstract

Wind-driven rain (WDR) modeling based on Lagrangian particle tracking (LPT) involves the trajectory simulation of raindrops released from a horizonal plane in the computational domain. Usually, the release location is determined in a tedious trial-and-error manner, which impairs the adoption of LPT method for WDR studies in terms of user's handiness and computational efficiency. In this study, the analytical solution for raindrop trajectories in an unobstructed domain are derived and presented. Based on the analytical solution, the location and sizes of the release plane can be easily determined a priori. A constant scaling factor can be further introduced to address possible obstruction effects by buildings. Unnecessary and expensive repetition of simulations to search for a proper release plane can be avoided, especially for scenario studies involving multiple raindrop sizes. In this paper, the accuracy, efficiency and effectiveness of the proposed automatic selection of release plane based on the analytical solutions are demonstrated based on selected case studies. It is deemed that the proposed innovative procedure for the determination of an effective and appropriate release plane can promote the widespread adoption of LPT approach for WDR studies.

Keywords: wind-driven rain, Lagrangian particle tracking, raindrop trajectory, CFD

*Corresponding author
Email address: `kendrick_tan@ihpc.a-star.edu.sg` (Kendrick Tan)

Preprint submitted to Journal of Wind Engineering and Industrial Aerodynamics March 3, 2023

1. Introduction

Wind driven rain (WDR) studies are widely conducted to address the impact of rainfall on building structure damage as one of the moisture sources for hygrothermal analysis (Choi, 1993, 1994, 1999, 2000; Blocken and Carmeliet, 2004; Van Hooff et al., 2011; Blocken, 2015; Briggen et al., 2009; Blocken and Carmeliet, 2002, 2007; Abuku et al., 2009; Tang and Davidson, 2004; Hangan, 1999; Ge et al., 2017; Foroushani et al., 2014). Extensive R&D efforts has also been channeled to study the effect of WDR on soil loss and rainsplash detachment(Erpul et al., 2003). In tropical countries such as Singapore, WDR has received increasing attention for safety concerns in building designs (BCA, 2015) due to the wetting induced by the infiltration of rain into occupational or transit areas. For the design of green and sustainable buildings in Singapore, WDR control becomes one of the critical performance-based design feature primarily due to the high frequency of rainfall in the tropical region (BCA, 2015). In addition, mitigation measures are expected to be implemented to minimize the safety risks imposed by WDR (Ooi et al., 2020).
Multiple methods have been developed to study the impacts of WDR. Semi-empirical models, as instructed in ISO 2009 (Blocken and Carmeliet, 2004), were recommended for WDR studies in UK or European countries with similar rainfall and weather conditions. The standard provides users with an approach to analyze hourly weather data (such as the wind speed, wind direction and horizontal rainfall intensity) to estimate the magnitude of WDR striking a building facade or wall of a stipulated orientation. On-site measurement of rain collected on the façade of interest is also commonly adopted to characterize the impacts of WDR. Over the past two decades, numerical modelling of WDR impact has been well researched. Both the Eulerian-Lagrangain approach (Choi, 1997; Lakehal et al., 1995; Etyemezian et al., 2000) and Eulerian-Eulerian approach (Kubilay et al., 2015a; Derome et al., 2017; Kubilay et al., 2013; Blocken et al., 2007) have been extensively explored to accurately simulate WDR impacts, particularly in the calculation of catch ratio on a façade of interest. Details about the differences between on-site measurements, semi-empirical models and CFD-based numerical models are well addressed by Blocken and Carmeliet (Blocken and Carmeliet, 2004).
In principle, the Eulerian-Lagrangian approach is an ideal method to trace the trajectory of a dilute water phase in the continuum of airflow. In the Eulerian-Lagrangian based procedure, raindrops are released from an elevation high above and upstream of the area of interest in the computational

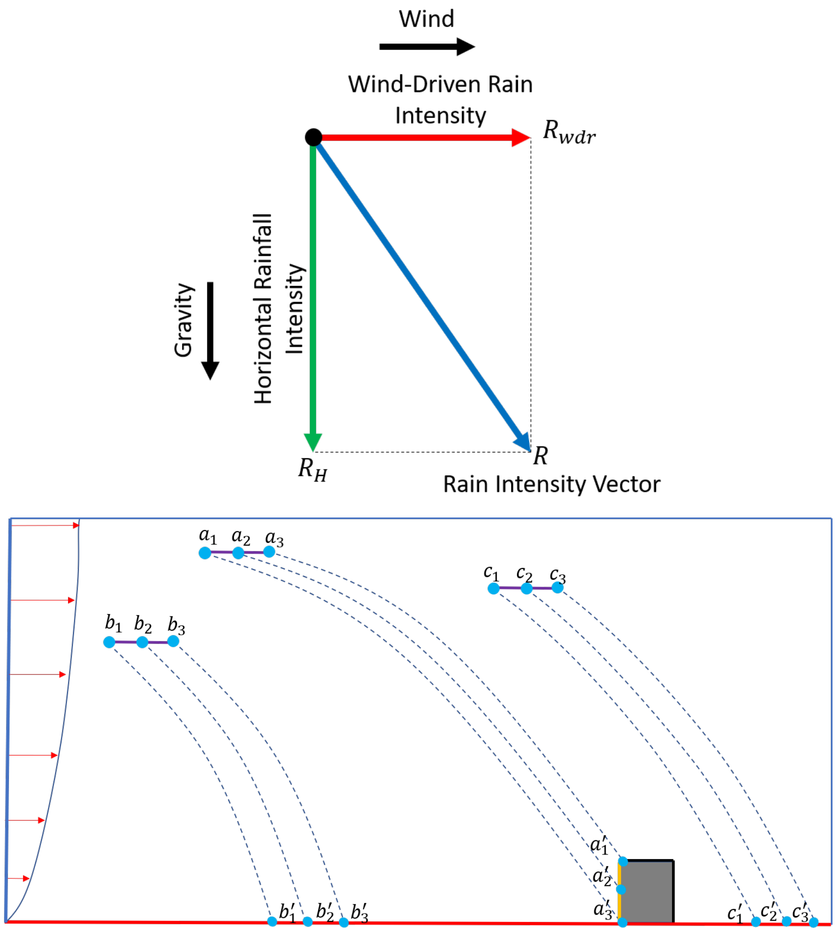

Figure 1: Trajectories of raindrops released from different locations.

domain. When subjected to external forces such as the aerodynamic drag forces and gravity, the trajectory of these raindrops are then numerically traced in an Eulerian-Lagrangian solution procedure. To better address the impact of WDR on a targeted region, it is expected that the targeted region should be fully and sufficiently covered by the falling raindrops. The working principle is illustrated in Fig. 1.

To fulfil this requirement, it is possible to define a horizontal release plane across the entire computational domain. However, such procedure will result in overly-expensive computations, especially when the simulation is conducted for a large scale and complex urban flow problem. Traditionally, a

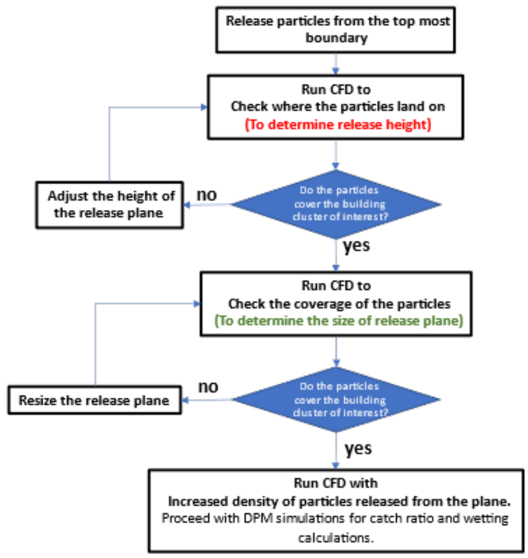

Figure 2: Flowchart for a conventional way of determining the release location in a trial-and-error manner.

search process, which is based on an iterative trial-and-error approach, is adopted to locate and subsequently size the horizontal plane for the release of raindrops. The iterative procedure is highlighted in the schematic shown in Figure 2. It is apparent that the search process for appropriate release plane complicates and imposes heavy computational demands when Lagrangian particle tracking approach is used for WDR studies.

To the best knowledge of authors, at least three to four iterations are typically required to obtain an effective release plane based on the conventional way as described earlier. The resultant effective release plane would be one within which the released raindrops would only land over the area of interest and/ or its vicinity. The manual search process is highly dependent on the user's domain knowledge and experience, and exacts a higher computational cost due to the need for iterated raindrop trajectories. Therefore, the search for an effective release plane becomes an inherent bottleneck which deters the widespread adoption of Eulerian-Lagrangian approach for WDR studies. In this study, the authors develop an innovative and efficient procedure to search for an optimally sized and located release plane such that the previously tedious and costly workflow can be greatly minimized or even avoided. An automatic selection of release plane procedure, based on an analytical

solution of raindrop trajectories within an unobstructed atmospheric boundary layer flow, has thus been developed.
In the following sections, the governing equations for WDR studies are first introduced, followed by an in-depth illustration of the innovative solution procedure for the automatic selection of release plane. The accuracy, efficiency and effectiveness of the proposed procedure will be further addressed in three test cases.

2. Governing Equations

2.1. Governing Equations for Urban Air Flow

In this paper, the study will be focused on steady-state incompressible flows under isothermal conditions. The two-equation $k-\epsilon$ model is adopted to address the effects of turbulence. The full set of Reynolds averaged Navier-Stokes equations is summarized as follows:
Conservation of mass

$$\nabla \cdot \mathbf{u} = 0 \tag{1}$$

Conservation of momentum

$$\frac{\partial \mathbf{u}}{\partial t} + \nabla \cdot (\mathbf{u}\mathbf{u}) = -\frac{1}{\rho_0}\nabla P + \nu_{eff}\nabla^2 \mathbf{u} + \mathbf{S_u} \tag{2}$$

where $\mathbf{u}$, P and t denote the air velocity, static pressure and time, respectively; ρ_0 represents the reference density; $\mathbf{S_u}$ is a source term for momentum equation. ν_{eff} is the effective turbulent kinematic viscosity, which is the sum of the laminar and turbulent kinematic viscosities.
In order to close the systems of governing equations, the transport equations for the standard $k-\epsilon$ model are adopted in this study, taking the form of
Transport equation for turbulent kinetic energy (k-equation)

$$\frac{\partial(\rho k)}{\partial t} + \nabla \cdot (\rho k \mathbf{u}) = \nabla \cdot [(\mu + \frac{\mu_t}{\sigma_k})\nabla k] + G_k - \rho\epsilon - Y_M \tag{3}$$

Transport equation for the dissipation rate of turbulent kinetic energy (ϵ-equation)

$$\frac{\partial(\rho \epsilon)}{\partial t} + \nabla \cdot (\rho \epsilon \mathbf{u}) = \nabla \cdot [(\mu + \frac{\mu_t}{\sigma_\epsilon})\nabla \epsilon] + C_{\epsilon 1}\frac{\epsilon}{k}G_k - \rho C_{\epsilon 2}\frac{\epsilon^2}{k} \tag{4}$$

where Y_M represents the contribution of fluctuating dilatation in compressible turbulence to the overall dissipation rate and G_k is the generation of k due to the mean velocity gradients, which is estimated from $G_k = \mu_t S^2$, $S = \sqrt{2S_{ij}S_{ij}}$, $S_{ij} = \frac{1}{2}(\frac{\partial u_i}{\partial x_j} + \frac{\partial u_j}{\partial x_i})$. The turbulence viscosity (μ_t) is calculated from $\mu_t = \frac{\rho C_\mu k^2}{\epsilon}$. σ_k, σ_ϵ, $C_{\epsilon 1}$ and $C_{\epsilon 2}$ are the set of empirical constants proposed for standard $k-\epsilon$ turbulence model (Versteeg and Malalasekera, 2007).

2.2. Raindrop Trajectories

Due to the small volumetric fraction of rain water in the air (less than 10^{-6}) for WDR simulations, it is a reasonable assumption that the raindrop trajectories are affected by the wind flow while the air flow is unaffected by the moving raindrops. In other words, the one-way coupling approach between the raindrops and air flow is usually adopted for WDR studies.
Suppose that the raindrops are spherically shaped with the rotational effects ignored, the raindrop trajectories are primarily affected by gravitational force and aerodynamic drag force exerted by the air flow. The transport of a raindrop is subject to the following set of ordinary differential equations:

$$\frac{d\mathbf{x_p}}{dt} = \mathbf{u_p} \tag{5}$$

$$m_p \frac{d\mathbf{u_p}}{dt} = m_p \mathbf{g} + \mathbf{F_D} \tag{6}$$

where subscript p refer to raindrop properties, ρ refers to density, $\mathbf{u}$ is velocity vector, m_p is the mass of the raindrop, $\mathbf{g}$ is the gravitational acceleration. The aerodynamic drag force (F_D) can be estimated as

$$\mathbf{F_D} = -\frac{\pi}{8}\mu_f Re C_d D_p (\mathbf{u_p} - \mathbf{u_f}) \tag{7}$$

where subscript f refer to the flow properties, Reynolds number (Re) is defined as $Re = \frac{\rho_f D_p |\mathbf{u_p} - \mathbf{u_f}|}{\mu_f}$, D_p and μ_f represents the raindrop diameter and the dynamic viscosity of air, respectively. The drag coefficient (C_d) for raindrop is determined based on the best-fit curve derived from the measurements by Gunn and Kinzer (Gunn and Kinzer, 1949), in the form

$$C_d = \begin{cases} \frac{24}{Re} & , Re \leq 0.1 \\ 10^Y & , Re > 0.1 \end{cases} \tag{8}$$

where $Y = \Sigma_{i=0}^{8} A_i X^i$, $X = log_{10}Re$. The relevant coefficients for the 8th-order polynomial function are as follows: $A_0 = 1.4114$, $A_1 = -0.9058$, $A_2 = 0.0847$, $A_3 = 0.0233$, $A_4 = -0.0034$, $A_5 = -0.0021$, $A_6 = 8.3387 \times 10^{-5}$, $A_7 = 1.1488 \times 10^{-4}$ and $A_8 = 1.1490 \times 10^{-5}$ (Segersson, 2003).
The formulae for raindrop drag coefficients were derived from the terminal velocities measured by Gunn and Kinzer. The curve fit relationship relating terminal velocities to raindrop diameters as developed by Van Mook (van Mook, 2002) are adopted in this study:

$$\mathbf{u_T} = 9.40 \times (1 - e^{-1570 \times d^{1.15}}) \tag{9}$$

Based on Eq. 9, the terminal velocities for the typical raindrops in tropical regions (BCA, 2015) are tabulated in Table 1. It is assumed that the gravitational acceleration rate is vertically along -z direction.

Raindrop Diameter [mm]	**Terminal Velocity (U_T) [m/s]**
0.5	-2.0
1.0	-4.0
2.0	-6.5
5.0	-9.0

Table 1: Terminal velocities of typical raindrops for rainfalls in tropical regions.

2.3. Log-law based Atmospheric Boundary Layer Flow

The incoming free stream for atmospheric boundary layer flow is usually assumed to follow log-law profile, as proposed by Richards & Hoxey (Richards and Hoxey, 1993). The velocity profile, and the corresponding k and ϵ profiles are described in following equations:

$$U(z) = \frac{u^*_{ABL}}{\kappa} ln(\frac{z + z_0}{z_0}) \tag{10}$$

$$k(z) = \frac{(u^*_{ABL})^2}{\sqrt{C_\mu}} \tag{11}$$

$$\epsilon(z) = \frac{(u^*_{ABL})^3}{\kappa(z + z_0)} \tag{12}$$

The ABL friction velocity (u^*_{ABL}) can be calculated based on the reference velocity (u_{ref}) which is measured at a reference height (z_{ref}) in the form of

$$u^*_{ABL} = \frac{\kappa u_{ref}}{ln(\frac{z_{ref}+z_0}{z_0})} \tag{13}$$

In the set of equations for atmospheric boundary layer flow, z_0 represents the aerodynamic roughness, κ and C_μ represents the von Kármán's constant and an empirical constant with a typical magnitude of 0.41 and 0.09 respectively.

2.4. Numerical Implementation in OpenFOAM

The proposed methodology for WDR studies in this paper is implemented in the well-known open source code – OpenFOAM framework. OpenFOAM v2012, which is maintained by ESI, will be adopted as the basic framework for our development. 2nd-order discretization schemes for temporal and spatial terms are used to approximate the partial differential or ordinary equations mentioned previously. The resultant algebraic equations are solved in a segregated solution procedure, as commonly implemented in OpenFOAM framework.

Steady-state airflows for the various test cases are obtained from the built-in flow solver – simpleFoam. A new solver, known as wdrLPTFoam, is created and implemented in OpenFOAM v2012 (OpenFOAM, 2012) together with the supporting drag library specific to raindrops. In the development framework for LPT solutions, raindrop trajectories can be readily obtained by executing a built-in utility command tool – steadyParticleTracks, based on the solution obtained from wdrLPTFoam. Erosion rates on the façade are also calculated and used as the marker to indicate the wetting area due to WDR (Lopez, 2014). Specific catch ratio can be post-processed based on the areas of the triangles with vertices formed from the initial and final location of the raindrops.

For brevity, this paper will be focused on an in-depth description of the automatic selection of release planes based on the analytical solutions for the unobstructed raindrop trajectories.

3. Automatic Selection of Release Plane

3.1. Analytical Solution for Raindrop Trajectory

The subsequent derivation of analytical solution for raindrop trajectories are subject to the following assumptions:

- Two-dimensional ABL flow is referenced to simply illustrate the derivation, with the assumed ABL flow traveling towards +x direction
- Raindrops travel vertically along the -z direction (direction of gravity) at a constant terminal velocity,U_T
- Raindrops follow the wind speed along the horizontal direction that is consistent with Log-law wind profile as shown in Eq. (10).
- Obstructions in the ABL flow are ignored

3.1.1. Vertical Location of raindrop, z

The vertical location of the raindrop at time t after its release can be denoted by z and it is given by

$$z = z_{rp} + \int_0^t U_T dt \tag{14}$$

where t denotes the duration that a raindrop travels in space upon release and and z_{rp} represents the vertical height at which the raindrop is released from.
One can then deduce the following relations: $z = z_{rp} + U_T t$, $t = \frac{z - z_{rp}}{U_T}$ and therefore

$$dt = \frac{1}{U_T} dz \tag{15}$$

3.1.2. Horizontal location of raindrop, x

The horizontal location of a raindrop at time t after its release is denoted by x. The derivation of x can be obtained based on the initial release location of the raindrop (x_{rp}).

$$x(z) = x_{rp} + \int_0^t U(z) dt$$

With reference to (x_{rp}, z_{rp}), the horizontal displacement of the raindrop upon its release is defined as

$$\Delta x(z) = x(z) - x_{rp} = \int_0^t U(z) dt \tag{16}$$

Substitution of Eq. (10) into Eq. (16) yields

$$\Delta x(z) = \frac{u^*}{u_T \kappa}\{(z+z_0)[ln(z+z_0)-1]-(z_{rp}+z_0)[ln(z_{rp}+z_0)-1]-(z-z_{rp})ln(z_0)\} \tag{17}$$

Equation (17) represents the horizontal displacement of a raindrop released from a location (x_{rp}, z_{rp}). Based on Equation (17), the expected landing location of a raindrop along the x direction (x_1) can be derived analytically as shown in the following:

$$\begin{aligned} x(z) &= x_1 \\ &= \Delta x(z) - \Delta x(z_1) \\ &= \frac{u^*}{u_T \kappa}\{(z+z_0)[ln(z+z_0)-1]-(z_{rp}+z_0)[ln(z_{rp}+z_0)-1]-(z-z_{rp})ln(z_0)\} \\ &- \frac{u^*}{u_T \kappa}\{(z_1+z_0)[ln(z_1+z_0)-1]-(z_{rp}+z_0)[ln(z_{rp}+z_0)-1]-(z_1-z_{rp})ln(z_0)\} \end{aligned}$$

The above equation can be further simplified as

$$x(z)-x_1 = \frac{u^*}{u_T \kappa}\{(z+z_0)ln(z+z_0)-(z_1+z_0)ln(z_1+z_0)ln(z_1+z_0)-(z-z_1)[ln(z_0+1)]\} \tag{18}$$

With reference to a known landing location of a droplet (x_1, z_1), the governing equation for the droplet trajectory is now a function of its arbitrary location (x, z) throughout its trajectory.

In particular, when the final location of the raindrop in the vertical direction is referenced as $z_1 = 0$,

$$x(z) - x_1 = \frac{u^*}{U_T \kappa}[(z+z_0)ln\frac{z+z_0}{z_0} - z] \tag{19}$$

Eq. (19) can be used to determine a suitable location for the release of a raindrop for it to land on a desired location.

3.2. Estimation of Raindrop Release Locations in Unobstructed Domains

The objective of this work is to determine a suitable release plane for the raindrops such that the released raindrops will land on the area of interest and/ or its vicinity. Upon determining this suitable release plane, closely spaced droplets can be released in a computationally cost-effective way to land on the area of interest for a better analysis of WDR impact.

The process of determining effective locations of release plane consists of two steps:

1. determining a suitable height for the release of raindrops
2. determining the dimensions of the release plane at this height

3.2.1. Release of raindrops from the top boundary of the computational domain

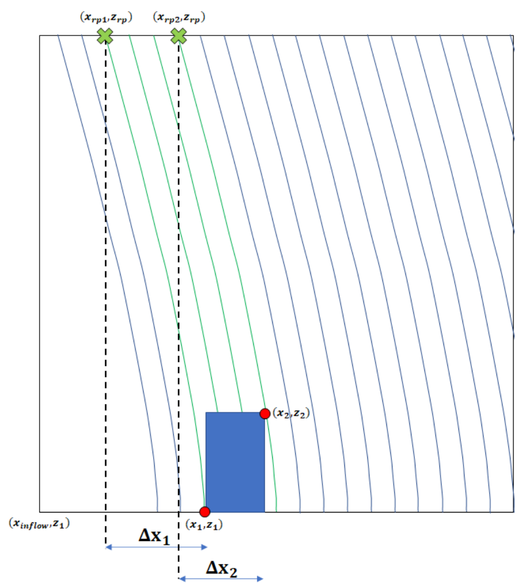

Figure 3: Trajectory of raindrops released at the top boundary of computational domain: Green line represents the trajectories of raindrops that landed onto the building

The droplets are usually released from the top surface for the sake of handiness and accuracy in computation as shown in Fig. 3.
The top boundary is a suitable location for the release of the raindrop if its horizontal displacement (Δx_1) of the raindrop (determined based on Eq. (19)) is lower than the fetching distance $dx = x_1 - x_{inflow}$ (where x_{inflow} is the x-coordinate of the upstream boundary of the computational domain) with reference to the lower bound of the region of interest.
Under such conditions, the final landing location of the raindrops can be estimated as the lower and upper bounds for the building of interest, which are denoted by Δx_1 and Δx_2, respectively.
Subsequently, the lower and upper bounds for release plane on the top boundary of the computational domain (at $z_{rp} = z_{top}$) can be determined as $(x_1 - \Delta x_1, z_{top})$ and $(x_2 - \Delta x_2, z_{top})$ respectively.

3.2.2. Release of raindrops from the plane within the computational domain

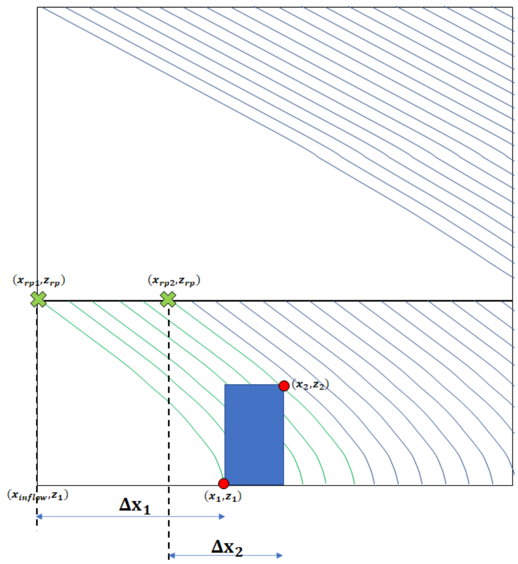

Figure 4: Trajectory of raindrops released at a height of z_{rp} and at the top boundary of computational domain: Green lines represents the trajectories of raindrops that landed onto the building.

For certain computational domain sizes and wind conditions, it may not be possible to define a release plane at the top boundary, i.e. $|x_1| > dx$ (as shown in Fig. 4). The raindrops released at the top boundary will not land onto the building of interest due to the flow conditions. Hence, the release plane should be defined at a lower height.
Assuming that a droplet released from (x_{rp1}, z_{rp1}) lands onto the lower bound of the region of interest at (x_1, z_1), we can set $\Delta x_1 = x_1 - x_{rp1}$. From Eq. (17), we can deduce that

$$\Delta x_1 = \frac{u^*}{U_T \kappa}\{(z_1 + z_0)[ln(z_1 + z_0) - 1] - (z_{rp} + z_0)[ln(z_{rp} + z_0) - 1] - (z_1 - z_{rp})ln(z_0)\}$$

The above equation can be simplified as

$$\eta[ln(\frac{ez_0}{\eta})] = \frac{\Delta x_1}{A} + z' ln(\frac{ez_0}{z'})$$

where $z' = z_1 + z_0$, $\eta = z_{rp} + z_0$, $A = \frac{u^*}{U_T \kappa}$ and e is the Euler's number
Further simplifications to the equation yields

$$\eta[\frac{E}{\eta}] = C \tag{20}$$

where $E = ez_0$ and $C = \frac{\Delta x_1}{A} + z'[ln(\frac{ez_0}{z'})]$
Eq. (20) is now a non-linear function with respect to η, which is a function of z_{rp}. Eq. (20) can be solved with an iterative Newton-Raphson method (Kelley, 2003) to obtain a solution for z_{rp}. In general, a solution may be obtained within 3 to 4 iterations.
Upon the solution of η, a height for the release of raindrops $z_{rp} = \eta - z_0$ may be obtained. Hence, the coordinates for the lower and upper bounds of the effective release plane can be determined based on the known z_{rp}.
It should be noted that when x_{rp} is defined as x_{inflow}, the mentioned procedure will compute the maximum allowable height of the release plane. Raindrops that are released at locations above this height may not land onto the area of interest (as shown in Fig 4).
For a droplet released from (x_{inflow}, z_{rp}), it is expected to land on the lower bound of the area of interest at (x_1, z_1). While the lower bound of the release plane is defined as (x_{rp1}, z_{rp}), its upper bound can be similarly determined based on Eq. (17), the known solution for z_{rp} and by setting $x = x_2$ and $z = z_2$. Upon which, we may obtain the coordinates for the upper bound of the release plane, (x_{rp2}, z_{rp}).
Once the release plane is appropriately positioned and sized, raindrops may be injected across the release plane into the computational domain for WDR studies. After which, the trajectory of the raindrops may be post processed for WDR analysis, such as to compute the catch ratio on a facade or to determine the wetting depth for the area of interest.

3.2.3. Summary of Procedure

Table 2 summarizes the overall procedure in determining the location and size of an effective release plane based on the analytical solution for a raindrop trajectory.

3.3. Determination of Release Plane in the Presence of Physical Bodies

Since the trajectory of a released droplet is predicted based on a flow domain without any physical obstructions, the effect of physical bodies on the

Conditions	Procedure
$\Delta x_1 \leq (x_1 - x_{inflow})$	Effective release plane can be defined on the top boundary, $z_{rp} = z_{top}$
	The lower bound of release plane, (x_{rp1}, z_{rp1}) is given by $(x_1 - \Delta x_1, z_{top})$.
	Compute Δx_2 based on $z = z_2$ and $z_{rp} = z_{top}$. The upper bound for release plane, (x_{rp}, z_{rp}) is given by $(x_2 - \Delta x_2, z_{top})$.
$\Delta x_1 > (x_1 - x_{inflow})$	It is necessary to set $z_{rp} < z_{top}$. Determine the maximum value for z_{rp} using Newton-Raphson method based on x_1 and z_1.
	The lower bound for release plane, (x_{rp}, z_{rp1}) is given by (x_{inflow}, z_{rp}).
	The upper bound for release plane, (x_{rp}, z_{rp2}) is given by $(x_2 - \Delta x_2, z_{top})$.

Table 2: Procedure to determine the release planes under different conditions.

droplet trajectory is not accounted for. Hence, the predicted trajectory of the rain droplets based on Eq. (17) may not be representative of the actual trajectory in the presence of physical bodies.

A scaling factor (SF) may be introduced to widen the area of interest over which the rain droplets will fall over. The addition of a scaling factor improves the recommended position and size of the release plane such that the released particles will fall over the area of interest and its vicinity. This ensures that the predicted trajectory of the released rain droplets will land onto the region of interest and/ or its vicinity despite any local flow deviations due to the presence of nearby physical boundaries.

The scaling factor is introduced to enlarge the release plane and therefore to offset any deviation in local wind speed induced by obstructions near the ground. Figure 5 illustrates how the scaling factor is used to enlarge the area of concern. The shifted bounds for the buildings will be used to determine the effective release plane for raindrops injection.

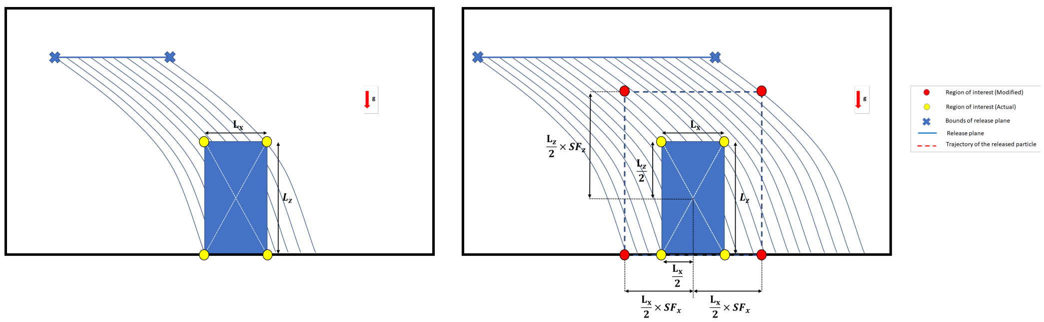

Figure 5: Shifted bounds of a building to account for the local flow changes due to obstructions near the ground

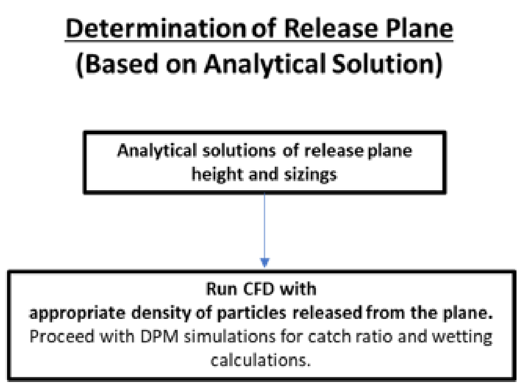

Figure 6: Schematic that contrasts the steps taken by the manual approach and the proposed approach

3.4. Summary of Procedures for the Selection of Release Plane

The previously tedious, manual and therefore expensive iterative procedure for determining an appropriate release plane (as illustrated in Figure 2) can be replaced by the proposed automatic approach based on the analytical solution of raindrop trajectories (as shown in Fig 6).

It is apparent that the simplified workflow is cost-effective, fast and automated. To the best experience of the authors, the conventional trial-and-error procedure typically requires at least 3 to 4 rounds of simulations or iterations before an appropriately sized and positioned release plane can be created. The mentioned procedure for release plane selection can efficiently reduce the computational demand by at least 75%. It should also be noted that the height and sizes of the effective release plane are highly dependent on the incoming wind speed, wind direction, raindrop diameter, surrounding buildings, building of interest, etc.

4. Case Study

In this Section, the effectiveness and robustness of the proposed automatic selection of release plane are demonstrated for WDR studies in three different test cases.

4.1. Demonstration on an Unobstructed ABL Domain

In this test case, a three-dimensional computational domain, 5000m in length, 100m in width and 500m in vertical height, has been created to model the urban flow without any internal obstruction. Standard two-equation $k-\epsilon$ model coupled with standard wall functions has been adopted to simulate the effects of turbulence. To satisfy the horizontal homogeneity, remedies to relevant empirical coefficients for standard $k - \epsilon$ model and standard wall function have been made (Blocken et al., 2007).

The log-law velocity profile (Richards and Hoxey, 1993) is used as an inflow boundary condition at the inlet at $x = 0m$ from $z = 0m$ up to the upper surface where $z = 500m$. The ABL velocity profile is defined based on the following parameters: $u_{ref} = 7.93m/s$, $h_{ref} = 4.0m$, $z_0 = 0.20354m$ and $\kappa = 0.42$. A zero normal velocity gradient is defined at the outlet boundary at $x = 5000m$. Symmetric boundary conditions are imposed on the two faces perpendicular to the y axis. Non-slip condition is imposed on the lower wall at $z = 0m$. The geometry of the computational domain is shown in Figure

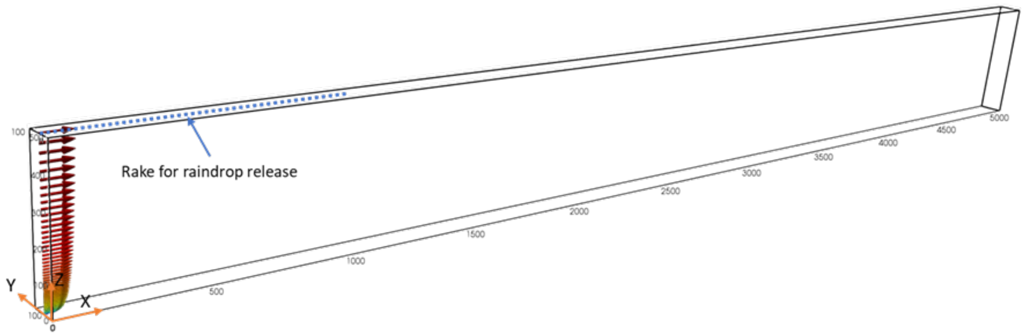

Figure 7: Three-dimensional computational domain for an unobstructed atmospheric boundary layer flow.

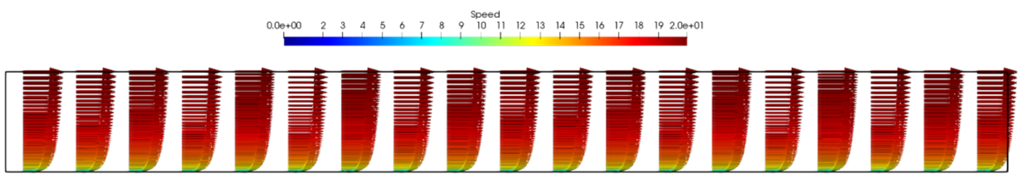

Figure 8: Vector plot of airflow across the computational domain.

7.
Due to the enforcement of homogeneity in the y-direction, the velocity profile of the flow remains unchanged in the streamwise direction as shown in Figure 8.
Trajectories of the raindrops released from the upper surface are simulated with wdrLPTFoam. wdrLPTFoam is a Lagrangian particle tracking solver that is developed for WDR studies based on the framework of OpenFOAM v2012 (OpenFOAM, 2012). For brevity, a 1000m-long streamwise rake is used to release eleven raindrops uniformly for raindrop trajectory study (as shown in Figure 7). Four types of raindrops (with diameters of 0.5mm, 1mm, 2mm and 5mm) are analysed for this case study. The simulation results are compared with the analytical solutions that was discussed earlier in this paper.
The comparison between the simulated and analytical results for the raindrop trajectories is shown in Figure 9. It is observed that the smaller droplets will travel further downstream. The trajectories of the released raindrops computed by the proposed analytical solution match well with that obtained from the wdrLPTFoam.

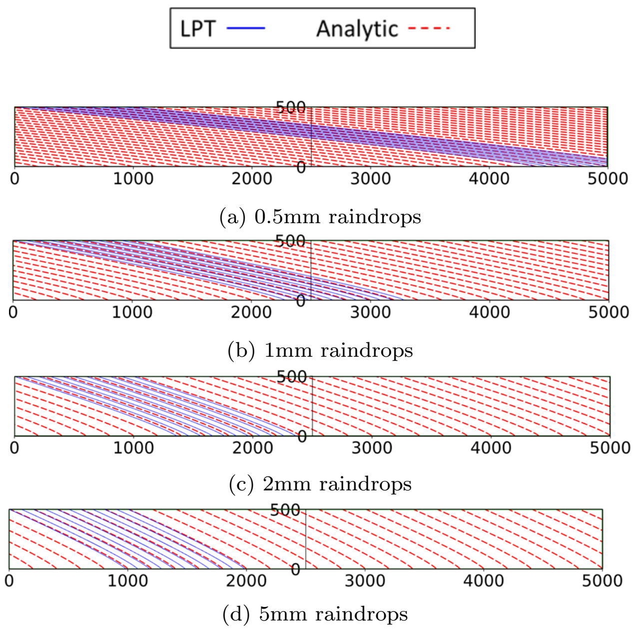

(a) 0.5mm raindrops

(b) 1mm raindrops

(c) 2mm raindrops

(d) 5mm raindrops

Figure 9: Comparison of raindrop trajectories between analytical and simulated solutions

The difference between the distance travelled by the raindrops predicted by our proposed method and by wdrLPTFoam can be quantified in terms of

$$Error = \frac{|\Delta x_{analytical} - \Delta x_{wdrLPTFoam}|}{\Delta x_{analytical}} \times 100\%$$

and the errors obtained for the different raindrop sizes are shown under Table 3.
A good agreement between these 2 sets of results implies that the analytical solutions proposed in the previous sections can be used to predict raindrop

Raindrop Diameter (mm)	$\Delta x_{analytical}(m)$	$\Delta x_{wdrLPTFoam}(m)$	**Error (%)**
0.5	4459.00	4384.29	1.68
1.0	2229.50	2274.40	2.01
2.0	1372.00	1356.46	1.13
5.0	990.90	997.52	0.67

Table 3: Error between the proposed analytical solution and numerical solution obtained from wdrLPTFoam

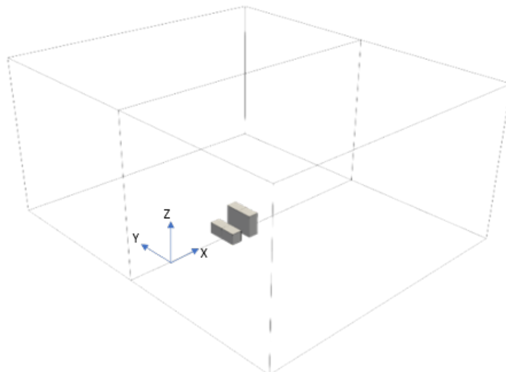

Figure 10: Computational domain for flow past two parallel buildings

trajectories in an unobstructed atmospheric boundary layer flow defined by a log-law inflow conditions (Richards and Hoxey, 1993).

4.2. Demonstration on an ABL Flow Over Two Parallel Buildings

WDR studies have previously been conducted for flows past two standalone parallel buildings (Kubilay et al., 2015b). Building 1 is 2m long (x), 6m wide (y) and 2.17m high (z), while Building 2 is located 2m downstream of Building 1. Building 2 is 2m long (x), 6m wide (y) and 4.29m high (z). This setup will be replicated in our computational study for the demonstration of our proposed procedure. The computational domain is 64m long (x), 64m wide (y) and 32m high (z) as shown in Figure 10. The dimensions of the bounding box for the 2 parallel blocks, (L_x, L_y, L_z) for this case study would be $(6, 6, 4.29)$m respectively.
ABL flow that is used for this study is characterised by parameters $U_{ref} = 3m/s$ at $h_{ref} = 2.4m$ and $z_0 = 0.49m$ along the (1,0,0) direction and (1, -1, 0) direction respectively. The gravitational acceleration acts along the (0,0,-1) direction.
Sensitivity study of the proposed selection of release plane towards various parameters are conducted. The computational study is subjected to changes in parameters such as the flow direction, scaling factor and the choice of the second bounding corner for the two parallel buildings of concern. It should be noted that the first bounding corner is always defined at the point on the upstream most section of the building on the ground. This allows users to define the effective release plane at the greatest height given the flow condi-

Flow Direction	Scaling Factor	Height of 2nd Bounding Corner	Coordinates of Effective Release Plane
(1,0,0)	1.0	$z_2 = 0$	Min: (-32.00, -3.00, 24.47) Max: (-26.00, 3.00, 24.47)
	1.0	$z_2 = \frac{L_z}{2}(1 + SF)$	Min: (-32.00, -3.00, 24.47) Max: (-23.22, 3.00, 24.47)
	1.2		Min: (-32.00, -3.60, 24.10) Max: (-21.60, 3.60, 24.10)
	1.5		Min: (-32.00, -4.50, 23.56) Max: (-19.15, 4.50, 23.56)
	2.0		Min: (-32.00, -6.00, 22.64) Max: (-14.99, 6.00, 22.64)
(1, -1, 0)	2.0	$z_2 = \frac{L_z}{2}(1 + SF)$	Min: (-30.00, 16.45, 27.89) Max: (-14.46, 32.00, 27.89)

Table 4: Selection of effective release planes for 1mm raindrops for the case of flow past 2 parallel blocks

tions and computational domain (as shown in Figure 4).
Table 4 summarizes the dimensions of the effective release planes during the parameter studies of the impact from 1mm raindrops on the two parallel buildings of concern. Based on the analytical solution, the maximum height of effective horizontal release plane reduces as the scaling factor increases. The larger scaling factor leads to relatively wider release plane. The use of the diagonal bounding corner remedied by scaling factor also effectively enlarges the release plane.

Simulation results based on respective effective release planes are shown in Figure 11 and 12. The parameter study shows that the raindrops released from the effective release plane will fall onto and in the vicinity of the two parallel buildings of concern.
As contrasted in Figure 11a and 11b, when the top downstream corner of the building is defined as the upper bound (x_2, z_2) instead of the downstream corner of the building at the ground level, a larger release plane is generated which results in a larger coverage of raindrops on the two buildings. Hence, the downstream top most point of a building is recommended to be defined as the upper bound (x_2, z_2) to improve the size of the effective release plane. As shown in Figure 11b, the effective release plane computed based on a

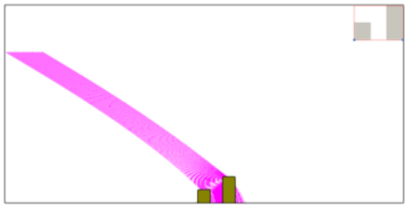

(a) $SF = 1.0$, $z_2 = 0$

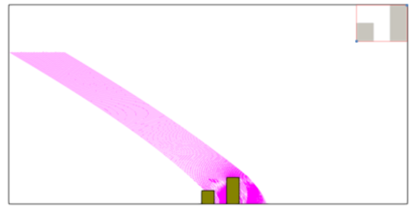

(b) $SF = 1.0$, $z_2 = L_z \times \frac{1+SF}{2}$

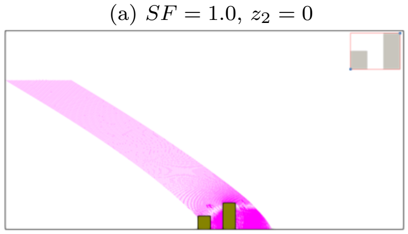

(c) $SF = 1.2$, $z_2 = L_z \times \frac{1+SF}{2}$

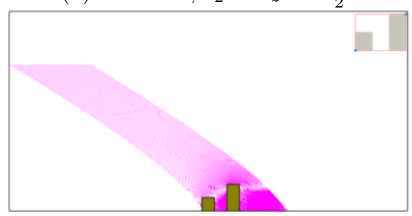

(d) $SF = 1.5$, $z_2 = L_z \times \frac{1+SF}{2}$

Figure 11: Trajectories of 1mm raindrops released from different release planes corresponding to various scaling factors and reference locations.

$SF = 1.0$ is not sufficiently large to release raindrops for a full coverage of the buildings. When SF is increased to 1.2, the release plane computed is widened and it leads to better coverage of the buildings by raindrops (as shown in Figure 11b).

When $SF = 2.0$ is used, the two buildings are enveloped within the raindrop trajectories (as shown in Figure 12a). In addition, it is observed that the proposed selection of release plane based on $SF = 2.0$ can lead to a satisfactory coverage over the buildings of interest for any arbitrary wind conditions (as shown in Figure 12b).

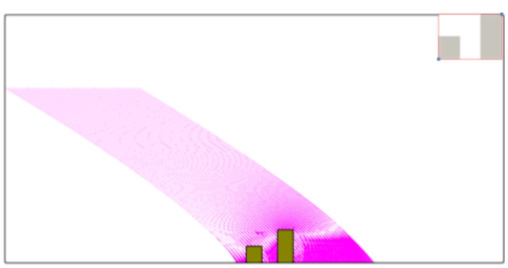

(a) Flow direction: $(1, 0, 0)$

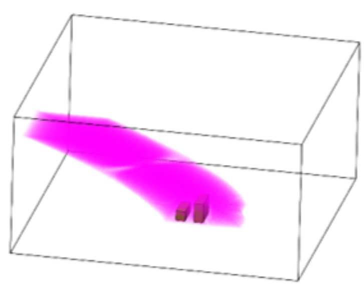

(b) Flow direction: $(1, 1, 0)$

Figure 12: Trajectories of $1mm$ raindrops released from release planes computed based on $SF = 2.0$ under different wind conditions.

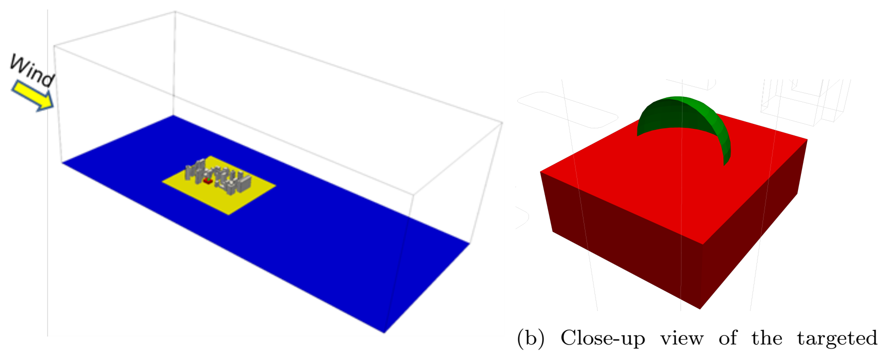

(a) Computational domain for the urban model

(b) Close-up view of the targeted building in the urban model

Figure 13: Geometry of a target building surrounded by a cluster of taller buildings

4.3. Demonstration on a Complex Urban Model with Surrounding Buildings

The third case study aims to demonstrate the effectiveness of our proposed method for the study of WDR on a building surrounded by a cluster of taller buildings. The complex urban model is generated based on a revised geometry model obtained from a standard tutorial case by OpenFOAM (OpenFOAM, 2012), named windAroundBuildings.

The building of interest, which consists of a brick-shaped base and a dome shelter on the roof, is the focus for the WDR study (as shown in Figure 13b). The computational domain for ABL flow around the buildings is generated and shown in Figure 13a.

The height of the tallest building ($79m$) is defined as a reference length to determine an appropriate size for the computational domain. This ensures that the boundaries of the computational domain are located sufficiently far from the cluster of buildings to avoid artificial acceleration of the flow (Blocken, 2015). The dimensions of the computational domain also comply with published guidelines for simulatations of flows in urban environments(Tominaga et al., 2008; Franke et al., 2007).

Table 5 summarizes the dimensions of the computational domain and the bounding box for the building of concern in this study. The geometrical information from Table 5 and the ABL flow conditions are the inputs required for the automatic selection of release plane proposed in this study.

WDR studies for the complex urban model have been performed based on ABL flows of varying speeds in the $(1, 0, 0)$ direction and the gravitational acceleration force acts in the $(0, 0, -1)$ direction. The case study of the buildings subjected to low-speed wind (based on an ABL flow parameters

Entity	Coordinates of Bounding Box
Building of Concern	Min: (90.1, 55.675, 0) Max: (116.7, 78.2, 15.8)
Computational Domain	Min: (-372, -210, 0) Max: (1000, 387, 456)

Table 5: Min and Max coordinates of the bounding box for the building of concern and the computational domain

Scaling Factor (SF)	Coordinates of Effective Release Plane
2.0	Min: (-372.00, 44.41, 209.95) Max: (-289.06, 89.46, 209.95)
5.0	Min: (-372.00, 10.63, 194.22) Max: (-166.56, 123.25, 194.22)

Table 6: Automatic selection of release plane for 1mm raindrops under low-speed wind conditions

of $U_{ref} = 3m/s$ at $h_{ref} = 2.4m$ and $z_0 = 0.49$) and high-speed wind (based on ABL flow parameters of $U_{ref} = 17m/s$ at $h_{ref} = 15m$ and $z_0 = 1.0$) is performed.
A sensitivity study of the SF for the proposed selection of effective release plane is also conducted. $SF = 2.0$ and $SF = 5.0$ are tested to examine the effect of varied SF of the release plane on the wetness for a surface of interest.

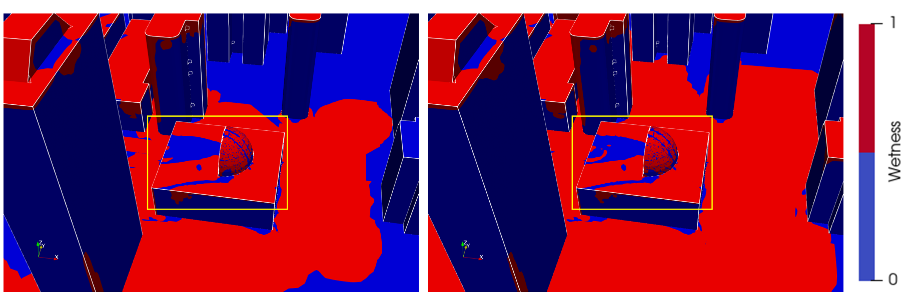

(a) $SF = 2.0$ (b) $SF = 5.0$

Figure 14: Surfaces wetted by raindrops injected from release planes based on different SF under low-speed wind conditions

Scale Factor (SF)	Coordinates of Effective Release Plane
2.0	Min: (-372.00, 44.43, 84.05) Max: (-234.03, 89.46, 84.05)
5.0	Min: (-372.00, 10.63, 78.13) Max: (-24.63, 23.25, 78.13)

Table 7: Automatic selection of release plane for 1mm raindrops under high-speed wind conditions

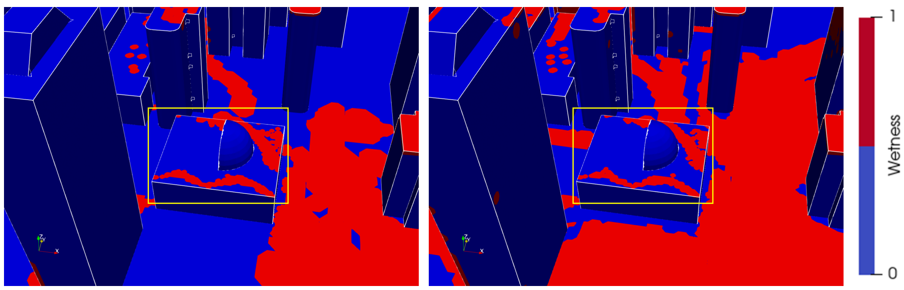

(a) $SF = 2.0$ (b) $SF = 5.0$

Figure 15: Surfaces wetted by raindrops injected from release planes based on different SF under high-speed wind conditions

Table 6 and 7 summarize the dimensions of the effective release planes for 1mm raindrops under different SF for the low-speed and high-speed wind conditions respectively. The raindrops are released at the same particle separation distance on the release plane for all the cases.

A wetness indicator that is based off an existing erosion modeling method in OpenFOAM (Lopez, 2014) is adopted for this paper. The original model computes the volume of material (Q) removed by a single abrasive particle of mass (m) and velocity (V).

A wetting indicator is similarly defined through a two-step process. First, Q_{wet} (which is modified from the variable Q defined in the erosion model) is computed where

$$Q_{wet} = \frac{mV^2}{K}(sin2\alpha - \frac{6}{K}sin^2\alpha) \qquad if\ tan\ \alpha \leq \frac{K}{6}$$
$$Q_{wet} = \frac{mV^2}{K}(\frac{Kcos^2\alpha}{6}) \qquad if\ tan\ \alpha > \frac{K}{6}$$

and K is the ratio of vertical to horizontal force components acting on the particle.

Based on the magnitude of Q_{wet} computed across all the surfaces within the computational domain, the wetness of the surfaces is defined in a binary format dependent on a threshold for Q_{wet} such that

$$
\begin{aligned}
wetness &= 0 \qquad && if\ Q_{wet} < \epsilon \\
wetness &= 1 \qquad && if\ Q_{wet} > \epsilon
\end{aligned}
$$

By setting an arbitrarily small value for ϵ, this wetness indicator returns 1 as long as a particle has landed on the surface. A threshold value of 2.2×10^{-13} for ϵ was found to be adequate in this work. While leveraging on the existing erosion model in OpenFOAM, this threshold indicates the presence or absence of raindrops on the surface.

In the visualizations for this work, the color blue is used to represent surfaces that are dry (given by $wetness = 0$), while red represents surfaces that are wet (given by $wetness = 1$).

The surfaces for the building of interest that are wetted by the raindrops injected from two release planes of different sizes for low-speed and high-speed wind conditions are illustrated in Figure 14 and 15 respectively.

The larger release plane (based on $SF = 5.0$) results in approximately 3 times as much computational cost compared to the release plane based on $SF = 2.0$. Despite the difference in sizes of the release plane due to varied SF, there are negligible differences in the wetted areas for the targeted building (2% and 0.3% for the low-wind and high-wind speed conditions respectively). Hence, the sensitivity study concludes that $SF = 2.0$ is adequate to determine a sufficiently large effective release plane for the analysis of WDR for this case study.

5. Conclusion

In this study, an innovative way for determining an effective horizontal release plane for Lagrangian particle tracking of raindrops in space has been proposed. The automatic selection of release plane is based on the analytical solution for unobstructed raindrop trajectories and a scaling factor to account for the impact of any physical obstruction. Parameter studies for various applications have demonstrated that the proposed procedure can effectively compute release plane locations that are accurate and economical for Eulerian-Lagrangian based WDR studies. Compared to conventional trial-and-error manner, the proposed method can provide users with at least

75% reduction in computational cost for the WDR studies.

Acknowledgment
This research project is supported by the National Research Foundation, Singapore, and Ministry of National Development, Singapore, under its Cities of Tomorrow R&D Programme (CoT Award COT-V4-2020-4). Any opinions, findings and conclusions or recommendations expressed in this material are those of the author(s) and do not reflect the views of National Research Foundation, Singapore and Ministry of National Development, Singapore.

References

Abuku, M., Blocken, B., Nore, K., Thue, J.V., Carmeliet, J., Roels, S., 2009. On the validity of numerical wind-driven rain simulation on a rectangular low-rise building under various oblique winds. Building and Environment 44, 621–632.

BCA, 2015. Bca green mark : Technical guide and requirements. GM NRB: 2015 .

Blocken, B., 2015. Computational fluid dynamics for urban physics: Importance, scales, possibilities, limitations and ten tips and tricks towards accurate and reliable simulations. Building and Environment 91, 219–245.

Blocken, B., Carmeliet, J., 2002. Spatial and temporal distribution of driving rain on a low-rise building. Wind and structures 5, 441–462.

Blocken, B., Carmeliet, J., 2004. A review of wind-driven rain research in building science. Journal of wind engineering and industrial aerodynamics 92, 1079–1130.

Blocken, B., Carmeliet, J., 2007. Validation of cfd simulations of wind-driven rain on a low-rise building facade. Building and Environment 42, 2530–2548.

Blocken, B., Stathopoulos, T., Carmeliet, J., 2007. Cfd simulation of the atmospheric boundary layer: wall function problems. Atmospheric environment 41, 238–252.

Briggen, P., Blocken, B., Schellen, H., 2009. Wind-driven rain on the facade of a monumental tower: numerical simulation, full-scale validation and sensitivity analysis. Building and Environment 44, 1675–1690.

Choi, E., 1994. Determination of wind-driven-rain intensity on building faces. Journal of Wind Engineering and Industrial Aerodynamics 51, 55–69.

Choi, E., 1997. Numerical modelling of gust effect on wind-driven rain. Journal of Wind Engineering and Industrial Aerodynamics 72, 107–116.

Choi, E.C., 1993. Simulation of wind-driven-rain around a building. Journal of Wind Engineering and Industrial Aerodynamics 46, 721–729.

Choi, E.C., 1999. Wind-driven rain on building faces and the driving-rain index. Journal of Wind Engineering and Industrial Aerodynamics 79, 105–122.

Choi, E.C., 2000. Variation of wind-driven rain intensity with building orientation. Journal of Architectural Engineering 6, 122–128.

Derome, D., Kubilay, A., Defraeye, T., Blocken, B., Carmeliet, J., 2017. Ten questions concerning modeling of wind-driven rain in the built environment. Building and Environment 114, 495–506.

Erpul, G., Norton, L., Gabriëls, D., 2003. The effect of wind on raindrop impact and rainsplash detachment. Transactions of the ASAE 46, 51.

Etyemezian, V., Davidson, C., Zufalla, M., Daia, W., Finger, S., Striegel, M., 2000. Impingement of rain drops on a tall building. Atmospheric Environment 34, 2399–2412.

Foroushani, S.S.M., Ge, H., Naylor, D., 2014. Effects of roof overhangs on wind-driven rain wetting of a low-rise cubic building: A numerical study. Journal of wind engineering and industrial aerodynamics 125, 38–51.

Franke, J., Hellsten, A., Schlünzen, K., Carissimo, B., 2007. Best practice guideline for the cfd simulation of flows in the urban environment-a summary, in: 11th Conference on Harmonisation within Atmospheric Dispersion Modelling for Regulatory Purposes, Cambridge, UK, July 2007, Cambridge Environmental Research Consultants.

Ge, H., Chiu, V., Stathopoulos, T., 2017. Effect of overhang on wind-driven rain wetting of facades on a mid-rise building: Field measurements. Building and Environment 118, 234–250.

Gunn, R., Kinzer, G.D., 1949. The terminal velocity of fall for water droplets in stagnant air. Journal of Atmospheric Sciences 6, 243–248.

Hangan, H., 1999. Wind-driven rain studies. a c-fd-e approach. Journal of Wind Engineering and Industrial Aerodynamics 81, 323–331.

Kelley, C.T., 2003. Solving nonlinear equations with Newton's method. SIAM.

Kubilay, A., Derome, D., Blocken, B., Carmeliet, J., 2013. Cfd simulation and validation of wind-driven rain on a building facade with an eulerian multiphase model. Building and environment 61, 69–81.

Kubilay, A., Derome, D., Blocken, B., Carmeliet, J., 2015a. Numerical modeling of turbulent dispersion for wind-driven rain on building facades. Environmental Fluid Mechanics 15, 109–133.

Kubilay, A., Derome, D., Blocken, B., Carmeliet, J., 2015b. Wind-driven rain on two parallel wide buildings: field measurements and cfd simulations. Journal of Wind Engineering and Industrial Aerodynamics 146, 11–28.

Lakehal, D., Mestayer, P., Edson, J., Anquetin, S., Sini, J.F., 1995. Eulero-lagrangian simulation of raindrop trajectories and impacts within the urban canopy. Atmospheric Environment 29, 3501–3517.

Lopez, A., 2014. LPT for erosion modeling in OpenFOAM.

van Mook, F.J., 2002. Driving rain on building envelopes. Techn. Univ., Fac. Bouwkunde.

Ooi, C., Ge, Z., Poh, H.J., Xu, G., 2020. Assessing effectiveness of physical barriers against wind-driven rain for different raindrop sizes. Engineering Analysis with Boundary Elements 111, 186–194.

OpenFOAM, O., 2012. The open source cfd toolkit user guide. OpenFOAM Foundation, Dordrecht .

Richards, P., Hoxey, R., 1993. Appropriate boundary conditions for computational wind engineering models using the k-ϵ turbulence model. Journal of wind engineering and industrial aerodynamics 46, 145–153.

Segersson, D., 2003. Numerical quantification of driving rain on buildings. SMHI.

Tang, W., Davidson, C.I., 2004. Erosion of limestone building surfaces caused by wind-driven rain: 2. numerical modeling. Atmospheric Environment 38, 5601–5609.

Tominaga, Y., Mochida, A., Yoshie, R., Kataoka, H., Nozu, T., Yoshikawa, M., Shirasawa, T., 2008. Aij guidelines for practical applications of cfd to pedestrian wind environment around buildings. Journal of wind engineering and industrial aerodynamics 96, 1749–1761.

Van Hooff, T., Blocken, B., Van Harten, M., 2011. 3d cfd simulations of wind flow and wind-driven rain shelter in sports stadia: influence of stadium geometry. Building and Environment 46, 22–37.

Versteeg, H.K., Malalasekera, W., 2007. An introduction to computational fluid dynamics: the finite volume method. Pearson education.